Ain Shams Engineering Journal (2016) 7, 47–56

Ain Shams University

Ain Shams Engineering Journal

www.elsevier.com/locate/asej
www.sciencedirect.com

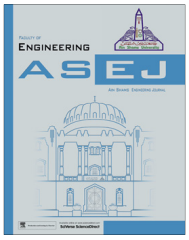

CIVIL ENGINEERING

Forecasting of meteorological drought using Hidden Markov Model (case study: The upper Blue Nile river basin, Ethiopia)

Mosaad Khadr *

Irrigation and Hydraulics Engineering Department, Faculty of Engineering, Tanta University, 31734 Tanta, Egypt

Received 12 June 2015; revised 10 October 2015; accepted 6 November 2015
Available online 10 December 2015

KEYWORDS

Drought;
Forecasting;
Stochastic modeling;
Blue Nile river basin

Abstract An improved drought management must rely on an accurate monitoring and forecasting of the phenomenon in order to activate appropriate mitigation measures. In this study, several homogenous Hidden Markov Models (HMMs) were developed to forecast droughts using the Standardized Precipitation Index, SPI, at short-medium term. Validation of the developed models was carried out with reference to precipitation series observed in 22 stations located in the upper Blue Nile river basin. The performance of the HMM was measured using various forecast skill criteria. Results indicate that Hidden Markov Model provides a fairly good agreement between observed and forecasted values in terms of the SPI time series on various lead time. Results seem to confirm the reliability of the proposed models to discriminate between events and non-events relatively well, thus suggesting the suitability of the proposed procedure as a tool for drought management and drought early warning.

1. Introduction

Drought is considered by many researchers to be the most complex but least understood of all natural hazards, affecting more people than any other hazard [1]. Drought is one of the major weather related disasters which is persisting over months or years. It can affect large areas and may have serious environmental, social and economic impacts. Globally, about 22% of the economic damage caused by natural disasters and 33% of the damage in terms of the number of persons affected can be attributed to drought [2]. These impacts depend on the severity, duration, and spatial extent of the precipitation deficit, as well as the socioeconomic and environmental vulnerability of affected regions [3]. Unlike the effects of a flood which can be immediately seen and felt, droughts build up rather slowly, creeping and steadily growing [4]. Droughts are typically classified into four types: meteorological, hydrological, agricultural and socioeconomic, and there are many drought indicators associated with each drought type [5,6]. Drought forecasting plays an important role in the mitigation of impacts of drought on water resources systems and water resources management [6–8].

* Tel.: +20 01069858309.
E-mail address: mosaad.khadr@f-eng.tanta.edu.eg
Peer review under responsibility of Ain Shams University.

ELSEVIER Production and hosting by Elsevier

http://dx.doi.org/10.1016/j.asej.2015.11.005

From a stochastic point of view, the problem of forecasting future values of a random variable can be seen as the determination of the probability density function of future values conditioned by past observations [9]. Yevjevich as reported in [10] was among the first at attempting a prediction of properties of droughts using the geometric probability distribution, defining a drought of k years as k consecutive years when there are no adequate water resources. Rao and Padmanabhan [11] investigated the stochastic nature of yearly and monthly Palmer's drought index (*PDI*) series to characterize them via valid stochastic models which may be used to forecast and to simulate the *PDI* series. Sen [12] derived exact probability distribution functions of critical droughts in stationary second order Markov chains for finite sample lengths on the basis of the enumeration technique and predicted the possible critical drought durations that may result from any hydrological phenomenon. Lohani and Loganathan [13] used *PDI* in a non-homogenous Markov chain model to characterize the stochastic behavior of drought and based on these drought characterizations an early warning system was used for drought management [14].

The main objective of this study is to build Hidden Markov Models (HMMs) for meteorological drought forecasting at short-medium term. The stochastic models presented in this study are based on SPI developed by McKee et al. [15] as drought index because there are a number of advantages arise from the use of the *SPI* index [14,16,17]. The primary advantage is that *SPI* is based on rainfall alone, so that drought assessment is possible even if other hydro-meteorological measurements are not available. The *SPI* is also not adversely affected by topography, it is defined over various timescales (3, 6, 9, …, 72 months) and this allows to use it as short, medium and long-term drought index to describe drought conditions over a range of meteorological, hydrological and agricultural applications. In particular, analytical expressions of *SPI* forecasts are derived as the expectation of future *SPI* values conditioned on past monthly precipitation, under the hypothesis of normally distributed precipitation aggregated at different timescales k. Validation of the model was carried out with reference to precipitation series observed in 22 stations located in the Upper Blue Nile River Basin (UBNRB), Ethiopia. To the best of our knowledge, the issue on forecasting of meteorological drought using Hidden Markov Model so far has not been addressed. Some of the other studies about using of Markov chain models to predict the transition from a class of severity to another are listed in [18–20]. The approach presented herein provides not only a stochastic methodology to forecast the transition probability from a drought class to another but also the magnitude and duration of drought event. It is hoped that the proposed approach and our findings obtained in this study are useful for further research in the area of drought forecasting.

2. Methods and materials

2.1. Study region and data

The Blue Nile river, which starts its flow from Lake Tana and ends at the Ethiopian–Sudan border, is the largest tributary of the Nile river in terms of discharge and annually contributes 60–69% of runoff to the Nile river at Khartoum [21,22]. The Blue Nile river originates in the highlands of Ethiopia, and the Upper Blue Nile River Basin (UBNRB) is the part of the watershed of the Blue Nile river basin which is under the Ethiopian territory (Fig. 1). The altitude of the UBNRB ranges from 511 m to 4052 m and the Blue Nile and its tributaries have a general slope toward the northwest, however the slopes are steeper in the east than in the west and northeast areas of the UBNRB (Fig. 1).

Forty-eight years (January 1960 to December 2007) of daily precipitation data from 22 meteorological stations in the upper Blue Nile basin were used in this study to forecast drought events. The selected stations represent a good spatial coverage across the study region (Fig. 1). Daily precipitation records were first processed in terms of data gaps using neighboring stations to fill in missing precipitation values and then converted to monthly values and after that homogeneity test was applied to the data using several homogeneity tests included absolute and relative homogeneity tests. The precipitation over the Blue Nile basin varies from 1000 mm in the north-eastern part to 1450–2100 mm over the south-western part of the sub-basin [23].

The mean annual areal rainfall over the UBNRB, within the studied period, is 1260 mm as shown in Fig. 2. The rainfall distribution is highly variable both spatially – decreasing from the southwest to the east and northeast – and temporally, i.e. over the yearly seasons. Moreover, as the rainfall over the UBRNB is highly seasonal, the Blue Nile river also possesses a strongly-varying seasonal flood regime, whereby over 80% of the annual discharge occurs during the four months from July to October. The average annual flow of the Blue Nile at the Sudan–Ethiopian border is about 48,660 million m^3 which represents more than 40% of Ethiopia's total surface water resources [24]. Hence, the UBNRB represents a substantial water resource for Ethiopia and as well for the downstream countries Sudan and Egypt.

2.2. Standardized Precipitation Index (SPI)

The Standardized Precipitation Index (*SPI*) is based on an equi-probability transformation of aggregated monthly precipitation into a standard normal variable and recommended by the World Meteorological Organization as a standard to characterize meteorological droughts [15,25,26]. The calculation of *SPI* requires that there are no missing data in the time series and the data record length is required to be at least 30 years [27,28]. McKee assumed an aggregated precipitation gamma distributed and used a maximum likelihood method to estimate the parameters of the distribution. In the most cases, the Gamma distribution is the distribution that best models observed precipitation data. Computation of the *SPI* involves the fitting of a gamma probability density function to a given frequency distribution of precipitation totals for a station [14,29]. The alpha and beta parameters of the gamma probability density function are estimated for each station, for each timescale of interest (1 month, 3 months, 12 months, 48 months, etc.) and for each month of the year.

After estimating coefficient alpha and beta the density of probability function is integrated with respect to, obtain an expression for cumulative probability that a certain amount of rain has been observed for a given month and for a specific timescale. The cumulative probability is then transformed into

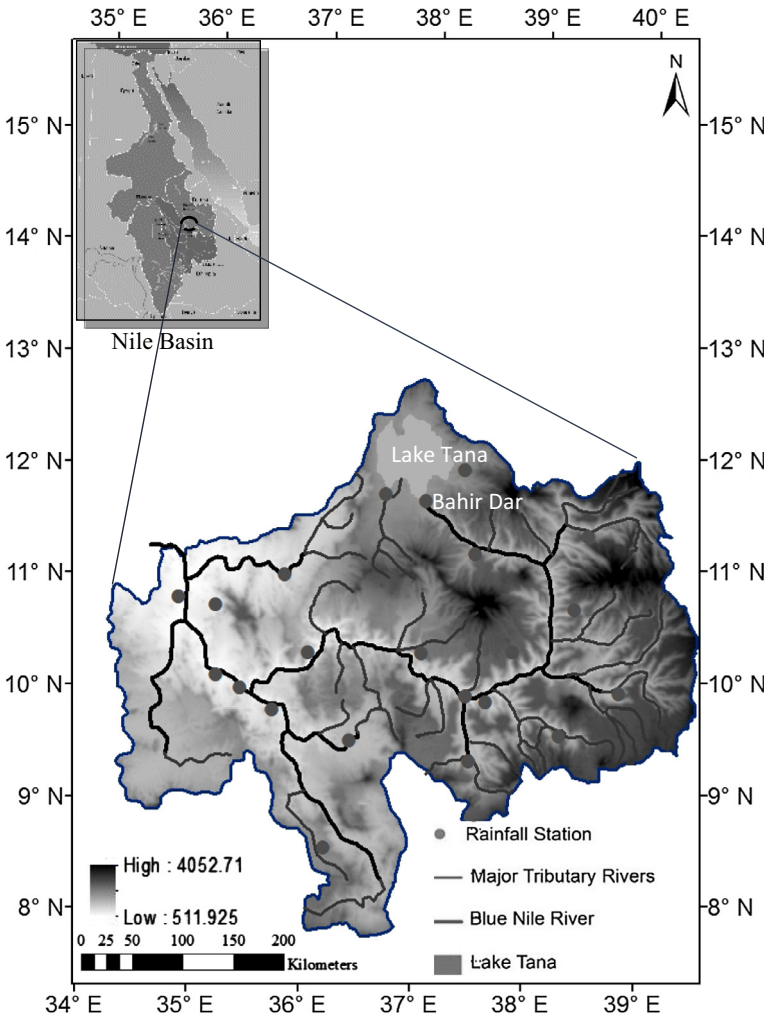

Figure 1 DEM of the upper Blue Nile river basin with locations of meteorological stations.

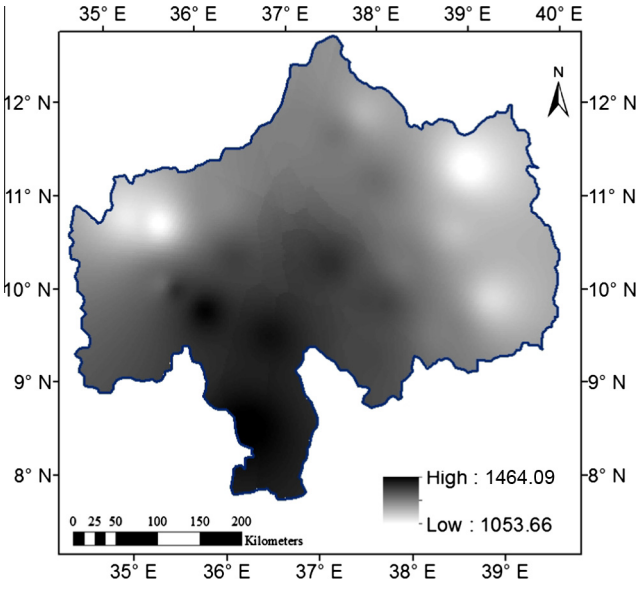

Figure 2 Mean annual precipitation (mm) over the upper Blue Nile river (1960–2007).

a normal standardized distribution with null average and unit variance from which we obtain the *SPI* index [30]. This approach, however, is neither practically nor numerically simple to use if there are many grid points or many station on which to calculate the *SPI* index. In this case, an alternative method was described in [31] using the technique that converts the cumulative probability into a standard. In addition, these various timescales can be useful in assessing effects on different components of the hydrological system (e.g., streamflow, reservoir levels and groundwater levels). In the present study, running series of total precipitation corresponding to 3, 6, 9, and 12 months were used and the corresponding *SPIs* were calculated: *SPI* 3, *SPI* 6, *SPI* 9, and *SPI* 12. The classification system shown in Table 1 is used to define drought intensities resulting from the *SPI* [32]. In this study SPI software Package, developed by the author [33], was used to compute time series of drought indices (*SPI*) for all stations.

2.3. Hidden Markov Model

The Markov chain is a probabilistic model used to represent dependences between successive observations of a random variable and it is based on the probability and statistics theory

Table 1 Weather classification based on the SPI index following McKee [15].

SPI values	Class
>2	Extremely wet
1.5 to 1.99	Very wet
1.0 to 1.49	Moderate wet
−0.99 to 0.99	Near normal
−1.0 to −1.49	Moderate dry
−1.5 to −1.99	Severely dry
<−2	Extremely dry

[34]. The Hidden Markov Model is a finite set of states, each of which is associated with a (generally multidimensional) probability distribution. Transitions among the states are governed by a set of probabilities called transition probabilities. In a particular state an outcome or observation can be generated, according to the associated probability distribution. It is only the outcome, not the state visible to an external observer and therefore states are "hidden" to the outside, hence the name Hidden Markov Model. The stochastic processes could be called an observable Markov model, when the output of the process is the set of states at each instant of time, where each state corresponds to a physical (observable) event [35].

Hidden Markov Models include the case where the observation is a probabilistic function of the state i.e. the resulting model is a doubly embedded stochastic process with an underlying stochastic process that is not observable (it is hidden), but can only be observed through another set of stochastic processes that produce the sequence of observations [36,37]. In Markov chain, the output at time t depends directly on the output at time $t-1$ however, in Hidden Markov Model the outputs are conditionally independent. The HMM is a useful tool to understand the statistics at local scale in terms of large-scale atmospheric patterns [38]. The concept of the *HMM* is an extension of that of the Markov chain and it consisted of a triple observed probability parameters (A, B, π) characterized by the following [39,40]:

(a) N, number of states, S_1 S_2, …, S_N. Although the states are hidden, for many applications from some physical consideration these states can be observed.
(b) M, the number of distinct observation symbols per state.
(c) The state transition probability distribution.

$$A = \{a_{ij}\} \tag{1}$$

where

$$a_{ij} = P[q_{t+1} = S_j / q_t = S_j] \quad 1 \le i,j \le N \tag{2}$$

(d) The observation symbol probability distribution in state j, $B = \{bj(k)\}$. B is named emission matrix where:

$$b_j(k) = P[v_k \text{ at } t / q_t = S_j] \quad 1 \le, j \le N; \quad 1 \le k \le M \tag{3}$$

$$V = \{v_1, v_2, \ldots, v_m\} \text{ which denote the individual symbols (observations)} \tag{4}$$

(e) The initial state distribution:

$$\pi_i = P[q_1 = S_i] \quad 1 \le i \le N \tag{5}$$

An application of HMM requires specification of two model parameters (N and M), and of the complete parameter set of the model three probability measures which is given by the following:

$$\lambda = [A, B, \pi] \tag{6}$$

A trellis diagram for a *HMM* with 4 states, shown in Fig. 3, could be used to visualize likelihood calculations of *HMMs*. Each column in the trellis shows the possible states of the weather at a certain time n. Each state in one column is connected to each state in the adjacent columns by the transition likelihood given by the elements $a_{i,j}$ of the transition matrix A as shown for state 1 at time 1 in Fig. 3. At the bottom is the observation sequence $X = \{x_1, \ldots, x_N\}$. $b_{i,k}$ is the likelihood of the observation $x_n = v_k$ in state $q_n = s_i$ at time n.

2.4. Performance measures

Several measures of goodness of fit were used to evaluate the forecast performance of all the aforementioned HMM models. The measures that were used include the following: Mean Absolute Deviations (*MAD*), the coefficient of determination (R^2), Root Mean Square Error (*RMSE*) and correlation coefficient (C_r). To investigate whether there is a significant difference between the mean from the observed and predicted data for various lead time, a Z-test for the means was employed in the analysis. The *MAD* measures the average magnitude of the errors in a set of forecasts, without considering their direction. It measures accuracy for continuous variables. Expressed *MAD* is calculated as follows:

$$MAD = \frac{\sum_{i=1}^{n} |SPI_{o_i} - SPI_{fi}|}{n} \tag{7}$$

where SPI_o is the observed value, SPI_f is the forecasted value and n is the number of data points.

In statistics, the coefficient of determination, R^2 is used in the context of statistical models whose main purpose is the prediction of future outcomes on the basis of other related information. The absolute fraction of variance, R^2, is calculated as follows:

$$R^2 = 1 - \frac{\sum_{i=1}^{n} (SPI_{o_i} - SPI_{fi})^2}{\sum_{i=1}^{n} (SPI_{o_i})^2} \tag{8}$$

With the variables already having been defined, the *RMSE* is the square root of the variance of the residuals. It indicates the absolute fit of the model to the data – how close the observed data points are to the model's predicted values. Whereas R-squared is a relative measure of fit, *RMSE* is an absolute measure of fit. Lower values of *RMSE* indicate better fit. *RMSE* is calculated as follows:

$$RMSE = \sqrt{\frac{\sum_{i=1}^{n} (SPI_{o_i} - SPI_{fi})^2}{n}} \tag{9}$$

The correlation coefficient a concept from statistics is a measure of how well trends in the forecasted values follow trends in past actual values (historical releases). The correlation coefficient is calculated as follows:

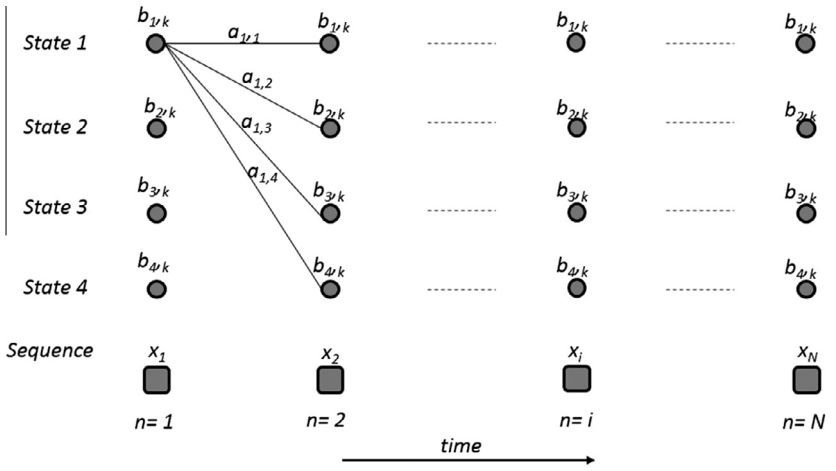

Figure 3 Trellis diagram shows the general architecture of four states HMM.

$$C_r = \frac{\sum_{i=1}^{n} SPI_{o_i} SPI_{fi} - \frac{\left(\sum SPI_{o_i}\right)\left(SPI_{fi}\right)}{n}}{\sqrt{\left[\left(\sum_{i=1}^{n} SPI_{o_i}^2 - \frac{\left(\sum_{i=1}^{n} SPI_{o_i}\right)^2}{n}\right)\left(\sum_{i=1}^{n} SPI_{fi}^2 - \frac{\left(\sum_{i=1}^{n} SPI_{fi}\right)^2}{n}\right)\right]}} \tag{10}$$

The *MAD* and the *RMSE* can be used together to diagnose the variation in the errors in a set of forecasts. To determine the time error and the best time of the forecasting, three following criteria were used [41–43]:

$$E_i = \frac{|SPI_{o_i} - SPI_{fi}|}{SPI_{o_i}} \tag{11}$$

$$F_i = \frac{\sum_{i=1}^{n} E_i}{i} \tag{12}$$

$$C_v = \frac{\left[\sqrt{\sum_{i=1}^{n} (E_i - \overline{E})^2}\right]}{\overline{E}} \tag{13}$$

where E_i is the relative error in month i, F_i is the average of cumulative relative error in the month i, $\overline{E}$ is the average of relative error, and C_v is the variation coefficient of relative error.

Relative Operating Characteristic (*ROC*), which is a graph that could be constructed for any event such as drought forecasting, was used to provide information on the hit rates and false alarm rates that can be expected from use of different probability thresholds to trigger advisory action. *ROC* is conditioned on the observations, answering the question given that an event Y occurred, what was the corresponding forecast? It therefore measures the ability of the forecasting system to discriminate between events and non-events, i.e. the resolution of the forecast. *ROC* is calculated by means of a 2×2 contingency table for each probability as in Table 2, which counts the number of forecast hits (*HT*), the number of misses (*MS*), the number of false alarms (*FA*) and the number of correct rejections (*CJ*). *ROC* is then probability of detection (*PoD*) as a function of the false alarm rate (*FAR*), where

$$PoD = \frac{HT}{HT + MS} \tag{14}$$

Table 2 2 * 2 contingency table for relative operating characteristic (ROC) calculation.

		Forecasted event	
		Yes	No
Observed event	Yes	Hit (HT)	Miss (MS)
	No	False alarm (FA)	Correct rejection (CJ)

$$FAR = \frac{FA}{FA + HT} \tag{15}$$

A *ROC* curve is plotted as a curve joining the *PoD* as a function of the *FAR* for all forecast probabilities. The area under the *ROC* curve gives a measure of the skill of the forecast.

3. Results and discussions

3.1. Computation of SPI at different timescales

The overall meteorological drought vulnerability in the UBNRB was assessed by reconstructing historical occurrences of droughts at varying time steps and drought categories with the SPI approach. A sample figure (Fig. 4) describing the *SPI* analysis is presented for Bahir Dar station which is situated on the southern shore of Lake Tana. Since the *SPI* in a 1-month timescale fluctuates between positive and negative values, detection of the start and end of a drought event is improper. Therefore, in this paper the *SPI* with 3, 6, 9, and 12-month timescales was used to identify drought events. Fig. 4 shows the changes in drought characteristics in frequency (time/month), duration (month) and magnitude of *SPI* for Bahir Dar station. Two recognizable severe dry periods were revealed, considering only the annual minimum spatially *SPI* value. The first period occurred during 1965 is characterized as an extreme drought event and the second period was during the 1980s is characterized as a severe drought for the whole area of UBNRB and reached its maximum value in 1984 [44].

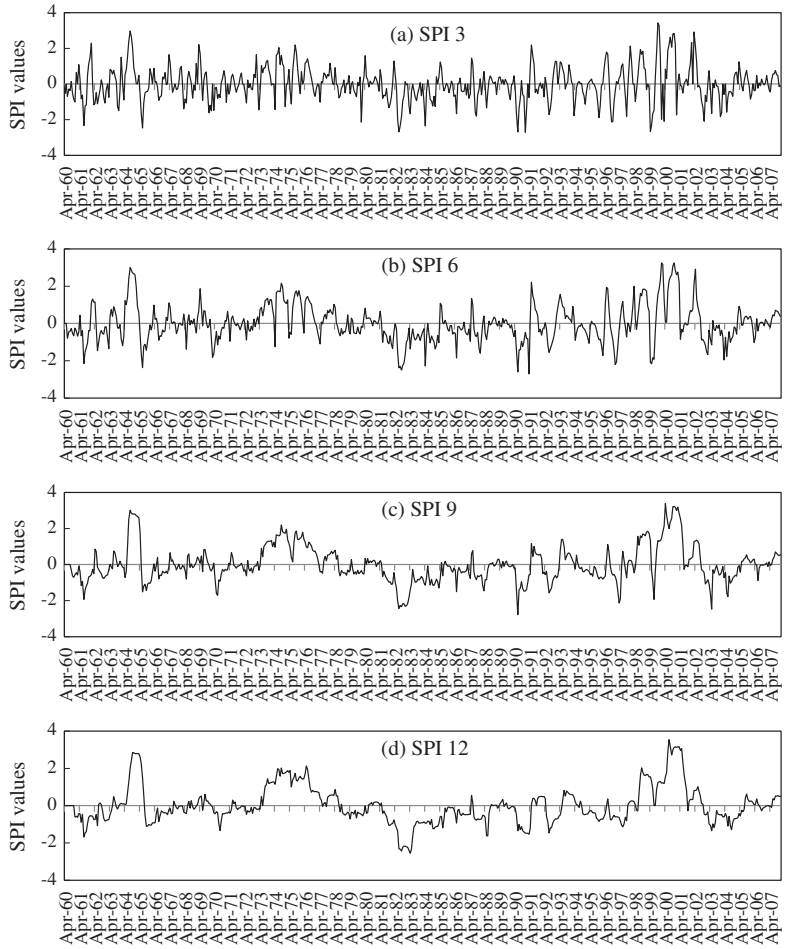

Figure 4 SPI time series based on the total monthly precipitation at Bahir Dar station (1960–2007). (a) SPI 3, (b) SPI 6, (c) SPI 9, (d) SPI 12.

3.2. Results of HMM

After the computation of the SPI index, drought and wet conditions were identified for the desired station in every month of every year on various timescale, then its relative frequency is obtained, and finally, using the Hidden Markov Model, drought was forecasted. One of significant advantages of *HMM* is that it can be estimated from sequences, without having to align the sequences first. The sequences used to estimate or train the model are called the training sequences, and any reserved sequences used to evaluate the model are called the test sequences. The data set from 1960 to 1993 was used to estimate model parameters, and the data set from 1994 to 2007 was used to validate the forecast using *SPI* 3, *SPI* 6, *SPI* 9, and *SPI* 12. In this paper, the proposed forecast models for *SPI* 3, *SPI* 6, *SPI* 9, and *SPI* 12 are presented for forecast lead times of 1, 2, 3, and 4 months.

A difficult problem when using *HMMs* is that of specifying the model in the first place. There are two parts to solve this problem; firstly the design of the structure i.e. what states there are and how they are connected, and secondly the assignment of parameter values, the transition and emission probabilities. Number of states of (*SPI*) S_1, S_2, …, S_7 from hydrological point of view are defined as follows: State 1 – Extremely wet, State 2 – Very wet, State 3 – Moderate wet, State 4 – normal state, State 5 – Moderate drought, State 6 – Severely drought, State 7 – Extremely drought. The suggested algorithm was tested on different models by varying the parameters over suitable ranges and choosing the values that give the minimum error between forecasted and actual *SPI* values. The model estimation was done with the forward-backward algorithm, also known as the Baum-Welch algorithm, which is described in [45]. The models were forecast one time step ahead and the subsequent result was used as an input in another model and forecast one time step ahead. All calculations reported in this paper were performed using MATLAB.

Transition probability matrices that illustrate how *HMM* can transfer from any one state to another, and emission matrices, that illustrate the sequence of these states, were calculated for each month based on the seven states of dry, normal and wet conditions; and for all *SPI* time steps, i.e. for *SPI* 3, *SPI* 6, *SPI* 9, and *SPI* 12. The final output time series was either 1, 2, 3 or 4 months ahead of the original time series. For each rainfall station, forecasts of *SPI* values were made using *HMM* for the various lead times. As an example, Fig. 5 shows the comparison between observed and forecasted SPI values for one of the 22 stations, namely Bahir Dar, for different combinations of the timescales.

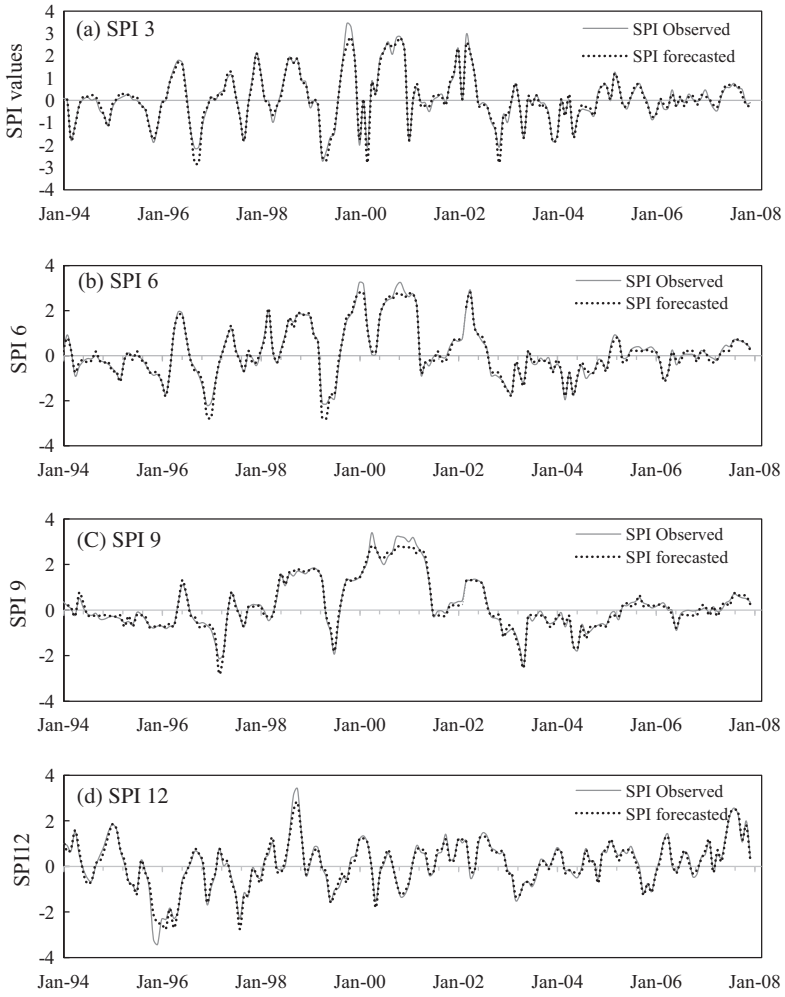

Figure 5 Model validation: comparison between observed and forecasted SPI for Bahir Dar station (1994–2007). (a) SPI 3, (b) SPI 6, (c) SPI 9, (d) SPI 12.

Table 3 shows the performance results for the set of *SPI* forecasts and illustrates the variation of R^2, *RMSE*, *MAE* and C_r for forecasting of the *SPI* with lead times of 1–4 months during the forecasting period at Bahir Dar station. The table shows that the forecasted values of the *SPI*, on various lead times, follow the calculated values very closely and preserve the basic statistical properties of the observed series. Table 3 indicates that the *RMSE*, for all models, is always larger or equal to the *MAD* which indicates that all the errors are of the same magnitude and high correlation between observed and forecasted values is obtained. For all models (SPI 3, SPI 6, SPI 9 and SPI 12) and for one month ahead R^2, *RMSE* is approximately the same and around 0.96, 0.20 respectively. All validation statistics in Table 3 show that, the more timescale is (3, 6, 9, and 12) the more accuracy in the higher lead time as scores are expected to decrease as lead forecast time increases. It is also known that the accuracy of weather forecasts decreases as the lead time increases to 2, 3, or 4 months.

The *Z*-test for the means was performed to investigate whether there is a significant difference between the mean from the calculated and forecasted *SPI* values on various lead times. Results of *Z*-test show that, the value the test static, *h*, equals 0 for all *SPI*, (3, 6, 9, 12, and for all lead times 1, 2, 3, 4) as presented in Table 3. The returned value of $h = 0$ indicates that, *Z*-test does not reject the null hypothesis that the observed and forecasted *SPI* come from a distribution with the same mean, at the 5% significance level. In addition, all calculated *z* values are between *Z*-critical values (± 1.96 for two-tailed at a 5% significance level).

In order to study the time changes of forecasting, the best forecasting time for the models was obtained by using Eqs. (11–13). Table 4 shows the minimum values of *E* and *F* indices, the corresponding month of occurrence of these values and the C_v index for forecasting period. Values of *E F* and C_v indexes in Table 4 show that there is no significant difference between SPI 3, SPI 6, SPI 9 and SPI 12 models. According to Table 4 and Fig. 6, the lowest rates of F_{min} index were in the First July, First June, First September and First July for SPI 3, SPI 6, SPI 9 and SPI 12 respectively. According to Fig. 6 and Table 4 it can be said that the monthly SPI values could be forecasted by HMM model about a 7 months ago with a good accuracy.

A *ROC* curve was plotted as a curve joining the *PoD* as a function of the *FAR* for all forecast probabilities. The area under the *ROC* curve gives a measure of the skill of the

Table 3 Comparison of statistical properties of the forecasted and observed data (1994–2007).

Time series		Mean	Std.	Min.	Max.	R^2	*MAD*	*RMSE*	Correl.	*Z* test	
										h	*z*
SPI 3	Observed SPI	0.091	1.047	−2.67	3.43	–	–	–	–	–	–
	1 month lead time	0.090	1.011	−2.749	2.801	0.965	0.137	0.196	0.982	0	0.002
	2 month lead time	0.116	0.967	−2.748	2.85	0.408	0.445	0.787	0.689	0	1.05
	3 month lead time	0.051	0.828	−2.750	2.84	0.154	0.600	0.940	0.495	0	0.239
	4 month lead time	0.163	0.852	−2.732	2.825	0.038	0.670	1.027	0.407	0	1.65
SPI 6	Observed SPI	0.107	1.072	−2.20	3.250	–	–	–	–	–	–
	1 month lead time	0.143	0.989	−2.80	2.80	0.955	0.136	0.2287	0.9791	0	−0.01
	2 month lead time	0.127	0.975	−2.80	2.92	0.552	0.356	0.691	0.769	0	−1.26
	3 month lead time	0.135	0.940	−2.80	2.85	0.532	0.420	0.707	0.753	0	−1.36
	4 month lead time	0.096	0.931	−2.80	2.87	0.548	0.483	0.694	0.757	0	−0.86
SPI 9	Observed SPI	0.122	1.071	−2.460	3.390	–	–	–	–	–	–
	1 month lead time	0.134	1.009	−2.77	2.90	0.963	0.135	0.2056	0.9820	0	−0.21
	2 month lead time	0.056	0.960	−2.76	2.80	0.809	0.298	0.455	0.900	0	−0.34
	3 month lead time	0.077	0.966	−2.80	2.80	0.603	0.373	0.655	0.790	0	−0.60
	4 month lead time	0.087	0.906	−2.80	2.80	0.573	0.475	0.680	0.766	0	−0.72
SPI 12	Observed SPI	0.131	1.022	−3.40	3.43	–	–	–	–	–	–
	1 month lead time	0.139	0.989	−2.752	2.800	0.970	0.128	0.179	0.985	0	0.004
	2 month lead time	0.054	0.929	−2.751	2.750	0.814	0.307	0.437	0.902	0	−0.18
	3 month lead time	0.099	0.974	−2.700	2.800	0.686	0.261	0.568	0.838	0	−0.74
	4 month lead time	0.137	0.893	−2.700	2.756	0.388	0.424	0.792	0.665	0	−1.21

Table 4 The minimum of *E* and *F* indexes and month of occurrence of them in forecasting period.

Time series	E_{min}	Month	$\overline{E}$	F_{min}	Month	C_v
SPI 3	0.0009	Second December	0.2827	0.1243	First July	0.7419
SPI 6	0.0018	Fourth July	0.2657	0.0656	First June	0.7593
SPI 9	0.0019	Fifth October	0.2511	0.1134	First September	0.7004
SPI 12	0.0009	Second November	0.2847	0.1673	First July	0.7436

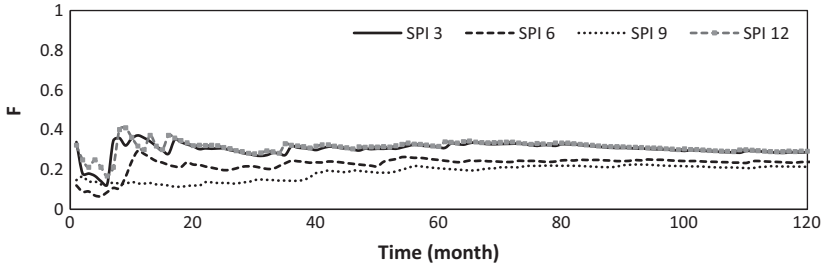

Figure 6 *F* index changes of models in forecasting period.

forecast. ROC curves for each threshold are shown in Fig. 7 for (a) *SPI*-3 and (b) *SPI*-6. For the *SPI*-3 and the *SPI*-6 for all thresholds the *ROC* curves are well above the no skill line indicating that the forecasting system does have some skill. The areas under the *ROC* curves, shown in Table 5, are greater than 0.5 indicating that the forecast has some skill. Table 5 indicates also that the *SPI*-6 forecast is more skillful than the *SPI*-3 forecast and that the forecasting system has potentially greater skill for the extreme events with more extreme thresholds for *SPI*. The *ROC* statistics suggest that the forecasting models are potentially skillful and able to discriminate between events and non-events.

4. Conclusion

Drought monitoring and forecasting are essential tools for implementing appropriate mitigation measures in order to reduce negative impacts of drought. Drought forecasting remains a difficult but vitally important task for hydrometeorologists and water resources managers. The availability of forecasts of drought indices, and the related confidence intervals for a given site, could be a helpful tool to the decision making process for drought mitigation. This paper described the procedure for drought forecasting using the Hidden Markov Model and its application in the upper Blue Nile river

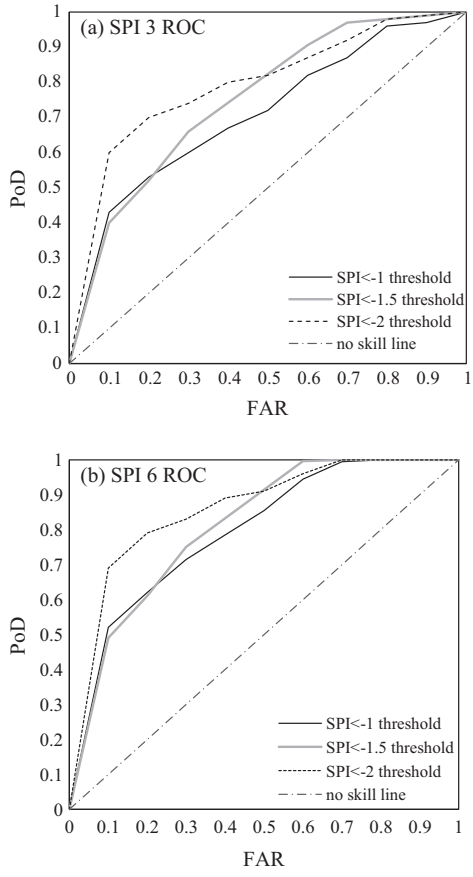

Figure 7 Relative operating characteristic (*ROC*) curves for forecasts of (a) *SPI* 3 and (b) *SPI* 6.

Table 5 Area under the relative operating characteristic (ROC) curves for SPI 3 and SPI 6.

	SPI < −1	SPI < −1.5	SPI < −2
SPI 3	0.7070	0.7492	0.7920
SPI 6	0.7936	0.8096	0.8574

basin in Ethiopia. Seven underlying hidden states that emit the visible observations were assumed using Standardized Precipitation Index (*SPI*). Validation of the model was carried out by comparing *SPI* values computed on precipitation observed in 22 stations in the upper Blue Nile river basin and the corresponding forecasts. Standard verification measures for probabilistic forecasts were used to assess the accuracy of the forecasts. The results of models performance indicate that the forecasted and observed data have similar characteristics in terms of the *SPI* time series on various lead time however, the accuracy of forecasting decreases as the lead time increases. Validation statics also indicate that the monthly SPI values could be forecasted by HMM model about a 7 months ago with a good accuracy. The analysis of the relative operating characteristics of the forecasting models showed that the developed models are able to discriminate between events and non-events relatively well. The overall conclusion of this analysis is that Hidden Markov Models could be used to forecast *SPI* time series of multiple timescales for more than one month ahead and could be used as an essential tools for medium-short term planning in the water resources management.

Acknowledgments

The Author would like to thank the Eastern Nile Technical Regional Office (ENTRO) for kindly providing data which were used for the analysis in this paper.

References

[1] Sivakumar MVK, Motha RP, Das HP. Natural disasters and extreme events in agriculture. Heidelberg (Berlin): Springer; 2005.
[2] Wilhite DA. Drought, a global assessment, natural hazards and disasters series, vol. 1. Routledge; 2000.
[3] European Commission JRC. European drought observatory; 2008.
[4] Lehner B, Henrichs T, Döll P, Alcamo J. EuroWasser, model-based assessment of european water resources and hydrology in the face of global change; 2001.
[5] Bordi I, Sutera A. Drought monitoring and forecasting at large scale. Methods and tools for drought analysis and management. Spring; 2007.
[6] Valipour M. Use of surface water supply index to assessing of water resources management in Colorado and Oregon, US. Adv Agri Sci Eng Res 2013;3:631–40.
[7] Zamani AMR, Monadi M, Zarei H. Using a first order markov chain model and SPI index to forecasting, monitoring and zoning of meteorological drought case study: Chahar Mahal and Bakhtiari province, Iran. J Environ Res Develop 2013;8.
[8] Valipour M. Critical areas of Iran for agriculture water management according to the annual rainfall. Eur J Sci Res 2012; 84:600–8.
[9] Valipour M. Number of required observation data for rainfall forecasting according to climate conditions. Am J Sci Res 2012; 74:79–86.
[10] Dracup JA. Drought monitoring. Stoch Hydrol Hydraul 1991;5:261–6.
[11] Rao AR, Padmanabhan G. Analysis and modeling of palmer's drought index series. J Hydrol 1984;68:211–29.
[12] Sen Z. Critical drought analysis by second-order Markov chain. J Hydrol 1990;120:83–202.
[13] Lohani VK, Loganathan GV. An early warning system for drought management using the Palmer drought index. J Am Water Resour Assoc 1997;33:1375–86.
[14] Cacciamani C, Morgillo A, Marchesi S, Pavan MV. Monitoring and forecasting drought on a regional scale: Emilia-Romagna region. Netherlands: Springer; 2007.
[15] McKee TB, Doesken NJ, Kleist John. The relationship of drought frequency and duration to time scales. In: Proc. of 8th conf applied climatology, Anaheim, California; 1993.
[16] Antonino Cancelliere GDM, Bonaccorso Brunella, Rossi Giuseppe. Stochastic forecasting of standardized precipitation index. In: Proc. of XXXI IAHR congress, Seoul, Korea; 2005.
[17] Khadr Mosaad, Schlenkhoff Andreas. Meteorological drought forecasting using stochastic models. In: Proc. of the 34th world congress of IAHR, Australia; 2011.
[18] Paulo Ana A, Pereira Luis S. Prediction of SPI drought class transitions using Markov chains. J Water Resour Manage 2007;21 (10):1813–27.
[19] Tabatabaeezade Monirsadat, Arzany Mohama dhosein, Ghafary Golale. Forecasting drought by Markov chain (Case study: Ardakan City). In: 21st int cong irrig drain Tehran, Iran; 2011. p. 213–8.

[20] M ahangir Alam AT, Sayedur Rahman M, Saadat AHM. Monitoring meteorological and agricultural drought dynamics in Barind region Bangladesh using standard precipitation index and Markov chain model. Int J Geo Geosci 2013;12(3):511–24.
[21] Abu-Zeid MA, Biswas AK. River basin planning and management. UK: Oxford University Press; 1996.
[22] Conway D. From headwater tributaries to International River. Observing and adapting to climate variability and change in the Nile Basin. Glob Environ Change 2005;15:99–114.
[23] Nour-El-Din MM. Climate change risk management in Egypt: proposed climate change adaptation strategy for the ministry of water resources & irrigation in Egypt. In: UNESCO – Office, Cairo; 2013.
[24] Conway D. The climate and hydrology of the upper Blue Nile river. Geogr J 2000;166(1):49–62.
[25] Khadr M. Water resources management in the context of drought (an application to the Ruhr river basin in Germany). Germany: Shaker Verlag; 2011.
[26] Dutra FDGE, Wetterhall F, Pappenberger F. Seasonal forecasts of droughts in African basins using the standardized precipitation index. Hydrol. Earth Syst. Sci. 2013;17.
[27] Svoboda M. An introduction to the drought monitor. Drought Network News 2000;12.
[28] Wu H, Hayes MJ, Weiss A, Hu Q. An evaluation of the standardized precipitation index, the China-Z Index and the statistical Z-Score. Int J Climatol 2001;21:745–58.
[29] Keyantash J, Dracup J. The quantification of drought: an evaluation of drought indices. Bull Amer Meteor Soc 2002;83:1167–80.
[30] Lloyd-Hughes B. The long-range predictability of European drought. London: University College London; 2002.
[31] Wilhite Donald A, Sivakumar MVK, Wood Deborah A. Early warning systems for drought preparedness and drought management. In: Proceedings of an expert group meeting held 5–7 september, Lisbon, Portugal; 2000.
[32] Khadr M, Morgenschweis G, Schlenkhof A. Analysis of meteorological drought in the Ruhr basin by using the standardized precipitation index. In: International conference on sustainable water resources management (SWRM2009), Amsterdam – Netherland; 2009.
[33] European-Commission. Communication from the commission to the European parliament and the council, addressing the challenge of water scarcity and droughts in the European Union; 2007.
[34] Keilson J. Markov chain models-rarity and exponentiality. New York: Springer-Verlag; 1979.
[35] Elliott RJ, Aggoun L, Moore JB. Hidden Markov models: estimation and control. New York: Springer-Verlag; 1995.
[36] MacDonald IL, Zucchini W. Hidden Markov and other models for discrete-valued time series. 1st ed. London (New York): Chapman & Hall; 1997.
[37] Zucchini W, MacDonald IL. Hidden Markov models for time series: an introduction using R. Boca Raton: CRC Press; 2009.
[38] Mares Constantin, et al. A hidden Markov model for the Orsova discharge level in springtime. In: Proc. of BALWOIS 2008 – Ohrid, Republic of Macedonia; 2008.
[39] Buhlmann P, Wyner AJ. Variable length Markov chains. Ann. Stat. 1999;27:480–513.
[40] Steeb WH. The nonlinear workbook. 4th ed. New Jersey: World Scientific; 2008.
[41] Valipour M et al. Comparison of the ARMA, ARIMA, and the autoregressive artificial neural network models in forecasting the monthly inflow of Dez dam reservoir. J Hydrol 2013;476.
[42] Valipour M, Banihabib ME, Behbahani SMR. Monthly inflow forecasting using autoregressive artificial neural network. J Appl Sci 2012;12:2139–47.
[43] Valipour M, Banihabib ME, Behbahani SMR. Parameters estimate of autoregressive moving average and autoregressive integrated moving average models and compare their ability for inflow forecasting. J Math Stat 2012;8:330–8.
[44] Khadr M, Schlenkhof A. Analysis of spatial and temporal variability of meteorological drought vulnerability in the Blue Nile river basin. In: E-proceedings of the 36th IAHR world congress, The Hague, the Netherlands; 2015.
[45] Belayneh A. Short term and long term SPI drought forecasts using wavelet neural networks and wavelet support vector regression in the Awash River basin of Ethiopia. Anne de Bellevue (Quebec, Canada): McGill Universit; 2012.

Mosaad Khadr is an Assistant Professor in Irrigation and Hydraulics Engineering Department, Faculty of Engineering, Tanta University, Egypt. The author completed B. Sc. in Civil Eng. (Structural Engineering) in 1997, and M.Sc. in Civil Engineering in 2002, Irrigation and Hydraulic Engineering, Faculty of Engineering, Tanta University, Egypt. In 2011, he did Ph.D. in Water Resources Management, University of Wuppertal, Germany.